ELSEVIER

Physica B 253 (1998) 278–289

PHYSICA B

Analysis of grazing incidence X-ray diffuse scatter from Co–Cu multilayers

I. Pape[a], T.P.A. Hase[a], B.K. Tanner[a,*], M. Wormington[b,c]

[a] *Department of Physics, Durham University, South Road, Durham, DH1 3LE, UK*
[b] *Bede Scientific Inc, Suite G-104, 14, Inverness Drive East, Englewood, CO 80112, USA*
[c] *Department of Engineering, University of Warwick, Coventry, CV4 7AL, UK*

Received 15 July 1997

Abstract

Grazing incidence diffuse X-ray scattering data from a Co–Cu multilayer with stepped interfaces grown by molecular beam epitaxy on a copper silicide buffer on a silicon substrate has been analysed using a computer code based on a fractal interface within the distorted wave Born approximation. We have extended the theory to include the scattering from a stepped interface and have shown that a single set of structural parameters can be used to obtain an excellent agreement between simulation and experimental data taken under very different X-ray optical conditions. The symmetry of the diffuse scatter on rotation about the surface normal can be explained if it arises from step bunching at the ends of extensive flat terraces. These steps have a self-affine nature, enabling the fractal model to be used successfully.

Keywords: X-ray scattering; Magnetic multilayers; Terraced interfaces

1. Introduction

Although discovered in 1988 [1], the giant magnetoresistance (GMR) observed in multilayers of transition metals is still not understood. While the concept of two spin-dependent scattering channels provides a very good qualitative description of the phenomenon, it is unclear whether the magnitude of the GMR is determined by the roughness of the multilayer interfaces or by Fermi surface effects associated with the crystallographic texture. In particular, it is still not clear why the GMR in layers grown by molecular beam epitaxy (MBE) is usually lower than equivalent films grown by sputtering.

The copper–cobalt system, which exhibits extremely high values of GMR [2,3], has received much attention and has the important advantage that the systems are immiscible. Most studies of the correlation between interface roughness and GMR [4–6] have relied on specular reflectivity measurements that cannot distinguish between roughness and compositional grading. We have recently shown that measurement of the diffuse

* Corresponding author. Tel.: + 44 191 374 2137; fax: + 44 191 374 2111; e-mail: b.k.tanner@durham.ac.uk.

0921-4526/98/$ – see front matter
PII: S0921-4526(98)00395-0

X-ray scatter provides powerful insights into the interface structure of these systems. In collaboration with workers at the University of Leeds, we have measured the grazing incidence diffuse X-ray scatter and have shown that changes in spin-dependent scattering on annealing Co–Cu multilayers arise through metallurgical changes not associated with the multilayer itself [7]. The very substantial changes are associated with alloying of the top copper layer with the gold anti-oxidation cap, and no changes in the roughness of the copper–cobalt interfaces were observed. In multilayer systems of 3d transition metals such as Co–Cu, the scattering from such a gold cap has a crucial effect on the grazing incidence X-ray scattering [8].

In order to distinguish the Co–Cu interface scattering from that due to other interfaces, we have exploited techniques using anomalous dispersion to change the scattering factor difference between the 3d transition metal layers while having little effect on the scattering from other interfaces. Measurements were made at two X-ray wavelengths, one far from the absorption edge and the other, close to the absorption edge. In performing these measurements, we exploit a unique property of synchrotron radiation, namely that it has a continuous spectrum of slowly varying intensity. Thus by examining the scatter close to and away from the edge, the scattering from the multilayer interfaces can be identified. Consistency of wavelength was achieved between runs by measurement of the fluorescence yield and calibrating against the near-edge absorption structure of standard samples. During analysis, the data were corrected for the changing area of sample illuminated by the beam during the scan, the changing fraction of the scatter reaching the detector, beam spill-off due to small sample size and the decay of the electron beam current in the storage ring.

A high GMR has recently been reported in Co–Cu multilayers grown by MBE on silicon with a cobalt silicide buffer. Grazing incidence diffuse scatter studies showed that the diffuse scatter through the first superlattice Bragg position was strongly peaked close to the specular peak in transverse (specimen only) scans in reciprocal space [9] and this was interpreted as arising from roughness with long lateral correlation. As a function of specimen orientation with respect to the incident beam, the relative positions of specular and diffuse peaks changed sinusoidally with angle of rotation about an axis normal to the specimen surface. From this it was concluded that the interface was stepped. This paper presents a more detailed study of the scattering from such a stepped interface and compares the scattering observed under different X-ray optical conditions with the predictions of a theoretical model.

2. Experimental configuration

All experiments were performed on Co–Cu multilayers grown on polished, single crystal, silicon substrates oriented normal to the [1 1 1] direction. The silicon substrates were 1 mm-thick slabs, the films being grown on square 10 mm × 10 mm faces. All samples were grown at the University of Leeds in the VG80M MBE facility with a base pressure of 3×10^{-11} mbar. During deposition, the pressure remained below 1×10^{-10} mbar and in some cases, the sample was rotated at a rate of 1 Hz. The 20 period multilayers, nominally 11.5 Å Co/7 Å Cu, were grown on a 10 Å Cu layer, deposited directly on the silicon substrate at 150°C. This then formed a Cu_3Si compound on to which a 15 Å Au layer was deposited. Finally, a nominally 15 Å thick Au cap was laid to prevent oxidation of the top layer of copper. The data presented in this paper were taken on a single sample but is representative of all samples examined.

Grazing incidence X-ray scattering measurements were made using the two circle powder diffractometer on station 2.3 at the Synchrotron Radiation Source (SRS) at Daresbury Laboratory. A water cooled, double bounce, Si (1 1 1) monochromator was used to select the wavelength and in the geometry selected this gave a dispersion of 1.5×10^{-4} at a wavelength of 1.4 Å. With incident beam slits before the monochromator of 100 μm in height and 4 mm in width, this produced count rates of typically 10^8 c.p.s. at the sample. The width of the beam-defining slits as well as the slits before the detector were determined to an accuracy of 10 μm. Analyser slits immediately in front of the

detector were set to 100 μm, giving a measured instrumental resolution function in a detector scan which was Gaussian and of 40 arcsec at full width half height maximum (FWHM) [10]. Through use of a further set of anti-scatter slits, evacuation of the air path to the high dynamic range scintillation detector [11], which was itself encased in lead, we obtained an experimental background of 1 c.p.s. limited by scatter of the main beam within the air path around the specimen.

Four types of X-ray measurements were made. Specular ($\delta\phi = 2\delta\theta$) scans recorded the intensity as the detector is swept at twice the angular rate of the incidence angle and scanned parallel to the reciprocal space vector q_z. Off specular longitudinal diffuse ($\delta\phi = 2\delta\theta + \Delta\theta$) scans recorded the intensity of the diffuse scatter just below the specular ridge by scanning in the same way as in specular scans but with a slight offset in the sample angle. In reciprocal space, these trace out radial lines emanating from the 000 reciprocal lattice point. Transverse (q_y) scans in reciprocal space were recorded by fixing the detector and scanning only the specimen. Detector-only scans were also performed, the effect of which was to scan around the Ewald sphere in reciprocal space keeping the penetration depth of the X-rays into the sample constant.

Wavelengths were chosen close to (1.3801 Å) and away from (1.48 Å) the Cu absorption edge in order to enhance the scattering from the Co/Cu interfaces and distinguish it from the scattering of top surface and buffer layer interfaces. Although the contrast enhancement at the Co edge was potentially better than the Cu edge [10], this was offset by a higher intensity in the latter part of the spectrum. In addition, the presence of structure on the Cu absorption edge enabled us to calibrate wavelength accurately to one part in 10^4, which was conveniently very well matched to the monochromator dispersion [10].

3. Simulation technique

3.1. Specular scatter

The specular, or coherent, field in each layer can be expressed as the sum of two plane waves. One of these, the transmitted wave, travels towards the substrate while the other, the reflected wave, travels away from the substrate. From the continuity of the electric field and its normal derivative across each interface, Parratt's well-known recursion formula is obtained [12],

$$R_l = \frac{r_l + R_{l+1}\varphi_{l+1}^2}{1 + r_l R_{l+1}\varphi_{l+1}^2}. \tag{1}$$

Here, $R_l = E_{l,\mathrm{r}}/E_{l,\mathrm{t}}$ denotes the reflection coefficient of the multilayer below the lth interface, where $E_{l,\mathrm{r}}$ and $E_{l,\mathrm{t}}$ are the amplitudes of the reflected and transmitted waves just above the lth interface. The Fresnel coefficients for reflection and transmission at each interface are given by $r_l = (k_{z,l} - k_{z,l+1})/(k_{z,l} + k_{z,l+1})$ and $t_l = 2k_{z,l}/(k_{z,l} + k_{z,l+1})$, respectively. For the layer thickness d_l, the complex amplitude factor is given by the expression $\varphi_l = \exp(\mathrm{i}k_{z,l}d_l)$. The z component of the wave vector in the lth layer is given, according to Snell's law, by $k_{z,l} = k(n_l^2 - \cos^2\theta)^{1/2}$, where n_l is the refractive index of the layer and θ is the grazing angle of the incident X-ray beam.

For a semi-infinite substrate, it follows that $R_{N+1} = 0$. Thus, the reflectivity coefficient of the multilayer may be obtained by solving Eq. (1) recursively, starting at the substrate and working up. Finally, the reflected intensity is given by $I_s = I_0|R_0|^2$, where I_0 is the intensity of the incident X-ray beam.

Real interfaces are not ideally sharp, as described above, but possess both roughness and grading which tend to smooth the interface profile when averaged over large areas. The electric susceptibility across such an interface can be expressed as $\chi_l[z_l - \delta z_l(x, y)]$, where $\delta z_l(x, y)$ is a random variable that describes the deviation of the interface from its mean position. Provided the total interface width is not too large, we may use the distorted-wave Born approximation to determine the replacement, $\langle r_l \rangle$, for the Fresnel reflection coefficient in Eq. (1). After some mathematics we arrive at

$$\langle r_l \rangle \approx r_l \exp(-2\sqrt{k_{z,l}k_{z,l+1}}\sigma_{l+1}^2) \times \int_{-\infty}^{\infty} \mathrm{d}z\, g_l(z) \exp(2\mathrm{i}\sqrt{k_{z,l}k_{z,l+1}}z), \tag{2}$$

where we have assumed that $\delta z_{l+1}(x, y)$ possesses a Gaussian distribution with a standard deviation, σ_{l+1}, and zero mean. Here, $g_{l+1}(z) = \chi'_{l+1}(z)/\chi_l - \chi_{l+1})$ is the normalised first derivative of the local electric susceptibility across the interface. The exponential term following the ideal Fresnel reflection coefficient accounts for interface roughness and the Fourier integral takes into account the effects of grading. For a rough interface possessing an abrupt local change in $\chi'_{l+1}(z)$, the second term is equal to unity. However, if the transition is smooth, and can be approximated by an error function of width, $\sigma_{g,l+1}$, the second correction term is equal to $\exp[-2k_l k_{l+1})^{1/2}\sigma^2_{g,l+1}]$, which is identical to the roughness term. This is an important result as it clearly demonstrates the inability of specular reflectivity to distinguish between roughness and grading at an interface; they both damp the reflection coefficient as the angle of the incident X-ray beam is increased.

3.2. Diffuse scattering

The distorted-wave Born approximation not only allows us to calculate the effect of roughness and grading on the specular reflectivity, but also allows us to predict the intensity of diffuse scatter as a function of the scattering vector, $\boldsymbol{q}$. If we again assume Gaussian height distributions at each interface, then after some lengthy mathematics, we arrive at the following expression for the scattering cross-section, $S(\boldsymbol{q})$, for a multilayer

$$S(\boldsymbol{q}) = \frac{A'k^4}{16\pi^2}\sum_{l,\,l'=1}^{N}\sum_{i,i'=r,t}\sum_{j,j'=r,t} P_{l,i,j}P^*_{l',i',j'} \times \frac{e^{-[(q_{z,l,i,j})^2\sigma^2_l + (q^{*2}_{z,l',i',j'})\sigma^2_{l'}]/2}}{q_{z,l,i,j}q^*_{z',l',i',j'}} \times \int d\rho[e^{q_{z,l,i,j}q^*_{z,l'i'j'}C_{l,l'}(\rho)} - 1]e^{i\boldsymbol{q}\cdot\rho}, \quad (3)$$

where $A' = A/\sin\theta$ is the area of the specimen illuminated by an incident X-ray beam of area A. The factors $P_{l,i,j}$ are given by

$$P_{l,i,\,j} = \Delta\chi_l \bar{E}_{l,i}\bar{E}'_{l,j}\int_{-\infty}^{\infty} dz\, g_l(z)\exp iq_{z,l,i,j}z), \quad (4)$$

where $\Delta\chi_l$ represents the difference in the electric susceptibility of layers l and $l+1$, calculated sufficiently far from the interface so that the effects of grading, described by the function $g_l(z)$, can be neglected. The electric field components directly below the lth interface, namely $\bar{E}_{l,i}$ and $\bar{E}'_{l,i}$, are obtained by solving the specular problem (Eq. (2) separately for the incident wave vector, $\boldsymbol{k}$, and for the inverted exit wave vector, $-\boldsymbol{k}'$, respectively. The parameters $q_{z,l,i,j}$ denote the z-component of the scattering vectors $\boldsymbol{q}_{l,i,j} = \boldsymbol{k}'_{l,i} - \boldsymbol{k}_{l,j}$. Finally, the summation is taken over all interface combinations within the multilayer, and for both the transmitted (t) and reflected (r) components of the electric fields. Hence, the calculation of diffuse scatter from a multilayer is computationally very demanding as it generally involves a large number of terms [13,14].

The covariance functions $C_{l,l'}(\rho)$ contain all of the information about the morphology of individual interfaces and the way in which the morphology propagates from layer to layer. In order to calculate the diffuse scatter from a multilayer, particular forms of the covariance functions have to be assumed. The shape of the lth interface is described by the auto-covariance function $C_l(\rho)$ and is defined by

$$C_l(\rho) = \langle \delta z_l(0)\delta z_l(\rho)\rangle, \quad (5)$$

where ρ is a vector lying in the plane of the interface and $\langle\Lambda\rangle$ denotes a configurational average over all points in the interface. The random quantity $\delta z_l(\rho)$ is the local centre of the grading profile at a lateral position ρ with an RMS value $\sigma_l^2 = \langle C_l(0)\rangle$ and vanishing mean. In this work $C_l(\rho)$ is assumed to be the isotropic auto-covariance function introduced by Sinha et al. [15] namely

$$C_l(\rho) = \sigma_l^2 \exp[-(\rho/\xi_l)^{2H_l}], \quad (6)$$

where $\rho = |\rho|$. This describes the behaviour of a self-affine fractal interface with a cut-off determined by the correlation length ξ_l. Although this represents a particular class of morphology it is quite general in that it can describe both jagged and gently undulating interfaces depending on the Hurst parameter, H_l. This parameter is restricted to the region $0 < H_l \leqslant 1$ and defines the fractal dimension, $D_l = 3 - H_l$, of the interface.

In general, we not only have to consider the roughness of an individual interface, but also the way in which the morphology propagates through the multilayer. If correlations exist between different layers, a non-zero covariance function

$$C_{l,l'}(\rho) = \langle \delta z_l(0) \delta z_{l'}(\rho) \rangle \tag{7}$$

has to be assumed. Here δz_l and $\delta z_{l'}$ represent the local centres of the grading profile at the lth and l'th interfaces, located at z_l and $z_{l'}$, respectively.

Two particular forms of $C_{l,l'}(\rho)$ used in this work, the first of which is given by

$$C_{l,l'}(\rho) = \sigma_{l,l'}^2 \exp[-(\rho/\xi_{l,l'})^{2H}] \exp(-|z_l - z_{l'}|/\zeta), \tag{8}$$

where the parameters $\sigma_{l,l'}^2 = \sigma_l^2 + \sigma_{l'}^2$ and $\xi_{l,l'}^{2H} = (\xi_l^{2H} + \xi_{l'}^{2H})/2$ are defined by means of the RMS roughness σ_l and correlation length ξ_l of individual interfaces. The paramater ζ describes the tendency of the individual layers to replicate the substrate roughness and is the distance over which correlations between the fluctuations at the lth and l'th interfaces are damped by a factor of $1/e$. No correlations are present in the case $\zeta = 0$ and nearly perfect correlation exists when ζ is much larger than the thickness of the multilayer. The computation time for Eq. (8) scales as N^2; however, it is extremely useful as the effects of partial correlation and frequency-dependent replication of interface morphology can be investigated.

The second covariance function used can be written as

$$C_{l,l'}(\rho) = (\sigma_{u,l'}\sigma_{u,l'}\delta_{l,l'} + \sigma_{c,l}\sigma_{c',l'}) \exp[-(\rho/\xi)^{2H}] \tag{9}$$

where $\delta_{l,l'}$ is the Kronecker delta operator and is unity when $l = l'$ and zero otherwise. The RMS roughness $\sigma_l^2 = \sigma_{u,l}^2 + \sigma_{c,l}^2$ of the lth interface is defined in terms of an uncorrelated component $\sigma_{u,l}$, that does not replicate from layer to layer, and a correlated component $\sigma_{c,l}$, which replicates the morphology of the substrate perfectly. The correlation length and Hurst parameter are assumed to be identical for all interfaces. By using this particular form of $C_{l,l'}(\rho)$, we can rearrange Eq. (3) so that the number of computations scale linearly with the number of layers, N, in the sample. Generally, the computation time scales as N^2 which is very slow for a large number of layers.

The experimental geometry most widely used to measure the diffuse scatter defines the scattered wave vector by placing a long, narrow slit in front of the detector. Since the resolution of this arrangement is poor out of the scattering plane we have to integrate Eq. (3) over the y-component of the scattering vector. This procedure gives the following result,

$$S(q_x, q_z) = \frac{A'k^3}{8\pi} \sum_{l,l'=1}^{N} \sum_{i,i'=r,t} \sum_{j,j'=r,t} P_{l,i,j} P^*_{l'i',j'} \times \frac{e^{-[(q_{z,l,i,j})^2\sigma^2_l + (q^*_{z,l',i',j})^2\sigma^2_{l'}]/2}}{q_{z,l,i,j} q^*_{z,l',i',j'}} \times \int dx [e^{q_{z,l,i,j}q^*_{z,l',i',j'} C_{l,l'}(x)} - 1] e^{iq_x x}, \tag{10}$$

from which the diffusely scattered intensity, $I(q_x, q_z)$, may be calculated using $I_d(q_x, q_z) = I_0 A^{-1} S(q_x, q_z)\delta\theta$, where $\delta\theta$ is the angular acceptance of the detector slit in the scattering plane. Thus, what is measured is related to a one-dimensional, rather than a two-dimensional, Fourier transform of the covariance function. This is fine for isotropic rough surfaces as it essentially yields the same information, but may be misleading for anisotropic roughness.

The Fourier transform in Eq. (10) does not in general have an analytical solution and numerical techniques must be used to evaluate it. Hence, this becomes the rate determining step when modelling diffuse scatter. To optimise the calculation we have developed an efficient numerical approach. For the particular covariance functions used in this work we may expand the Fourier transform as a series, for example,

$$\int dx [e^{q_{z,l,i,j}q^*_{z,l',i',j'}\sigma^2_{l,l'} \exp[-(\rho/\xi_{l,l'})^{2H}]} - 1] e^{iq_x x} = 2 \sum_{n=1}^{\infty} \frac{q^{2n}_{z,l,i,j}(q^*_{z,l',i'j'})^{2n}\sigma^{2n}_{l,l'}}{n!} \xi_{l,l'} F(q_x \xi_{l,l'}/n^{1/2H}), \tag{11}$$

where in practice only the first few terms of the summation have to be considered and

$$F(q) = \int_0^\infty \mathrm{d}x\, \mathrm{e}^{-x^{2H}} \cos(qx). \tag{12}$$

Because the function $F(q)$ may be accurately tabulated in advance for various values of H this method is computationally much faster than evaluating Eq. (10) directly [16]. All the simulations shown in this paper have been performed using this second covariance function.

The model has been proven for the case of a single rough interface with an error-function grading profile by fitting the experimental data from a polished surface of the glass ceramic Zerodur[1] [17]. We have been able to separate the grading and roughness by measurement of the specular scan and one of the diffuse scans; all other diffuse scans being excellently fitted by the parameters derived from the former data sets.

4. Results

Fig. 1 shows the specular curve for one sample, corrected for the forward diffuse scatter measured in a -0.1° offset longitudinal diffuse scan ($\delta\phi = 2\delta\theta + \Delta\theta$), together with our best fit to a simulated curve. This latter curve has been simulated with a structure: Si (6 Å rms roughness), 15 Å Cu_3Si (6 Å rms roughness), 21.5 Å Au (6 Å rms roughness), {15.0 Å Co (6.5 Å rms roughness), 6.5 Å Cu (7.0 Å rms roughness)} $\times$ 19, 14.5 Å Co (6.5 Å rms roughness), 31 Å $Au_{0.8}Cu_{0.2}$ (7 Å rms roughness) (Fig. 2). It proved essential to use an Au–Cu alloy for the cap, suggesting that the top Cu layer of the nominally 20 period superlattice had interdiffused with the Au. When a pure Au cap was used in the simulation, the interference fringe period was correct but the positions of the maxima and minima were displaced from those observed experimentally. This sensitivity of the interference fringe positions to the position of the critical angle is a general effect in specular reflectivity curves and the fringe positions are therefore determined by the electron density at the surface. This change in surface density was noted in annealed Cu–Co multilayers grown on sapphire and high-angle X-ray diffraction experiments confirmed the presence of the alloyed surface layer [7].

Fig. 3 shows transverse scans taken through the 1st-order Bragg peak for different azimuthal angles where the specimen is rotated about the surface normal. We note the sharp peak in the diffuse scatter adjacent to the very narrow specular peak. There is a clear displacement of the diffuse scatter peak from the specular ridge and this is a strong

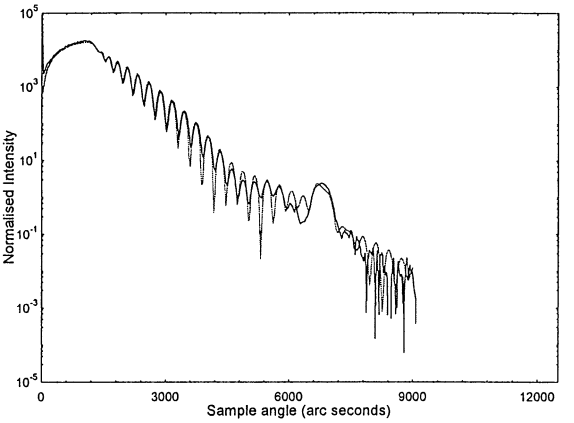

Fig. 1. Experimental and simulated reflectivity curves from a Cu–Co multilayer.

Layer thickness (± 1 Å)	Interface roughness (± 1 Å)	
$Au_{0.8}\ Cu_{0.2}$ (31 Å)	←7.0 Å rms	
Co (14.5 Å)	←6.5 Å rms	
Cu (6.5 Å)	←7.0 Å rms	x 19
Co (15 Å)	←6.5 Å rms	
Au (21.5 Å)	←6.0 Å rms	
Cu_3Si (15 Å)	←6.0 Å rms	
Si Substrate	←6.0 Å rms	

Fig. 2. Structure used to simulate the reflectivity curve in Fig. 3.

[1] Zerodur is a registered trademark of Schott Glaswerke, Mainz.

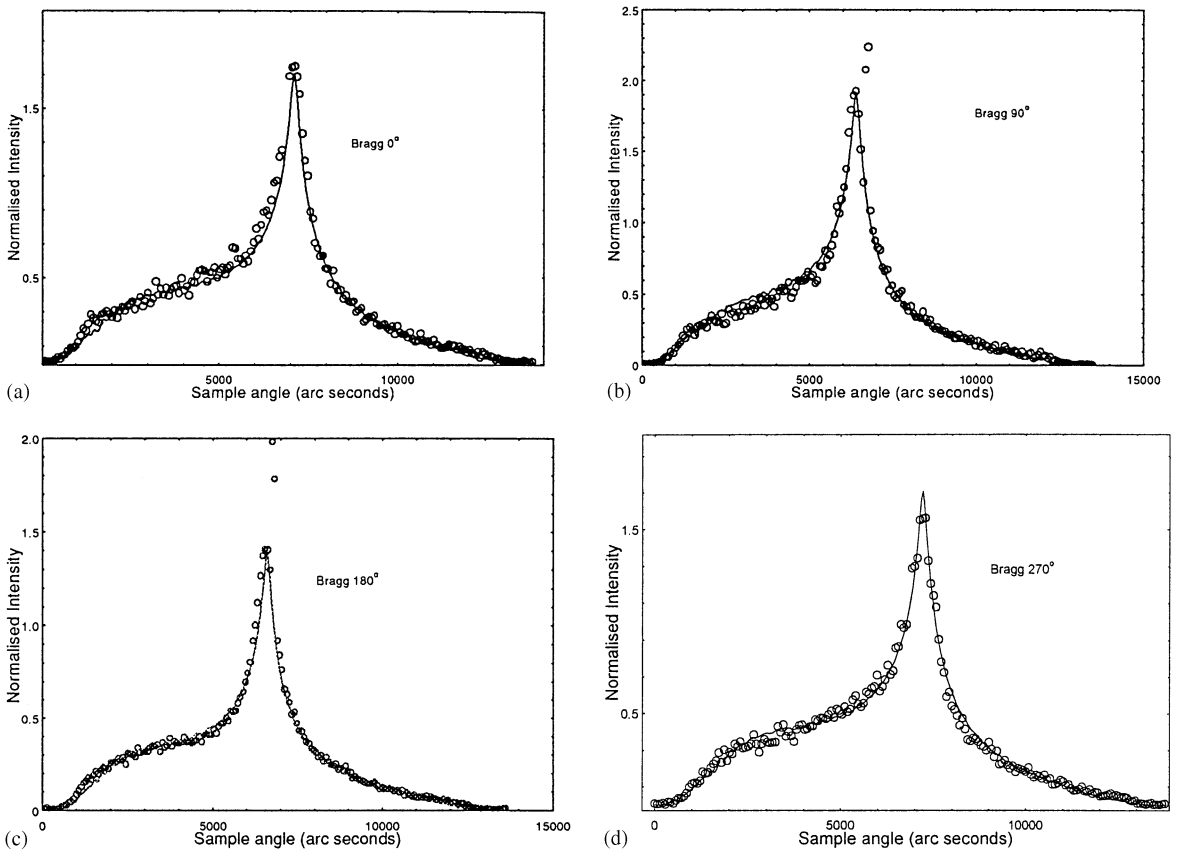

Fig. 3. Transverse diffuse scan taken through the first-order Bragg peak on rotation about the sample's surface normal.

function of the specimen orientation with respect to the incident beam. On rotation of the specimen about the surface normal, the relative position of the specular and diffuse scatter peaks reverses and the separation can be fitted well by a sine function (Fig. 4).

Asymmetries in scattered X-rays which are a function of the direction of the input beam ($+q_y$, $-q_y$, $+q_x$, $-q_x$) have been observed previously [18–21]. In all cases they have been ascribed to a preferential direction on the surfaces and often, by implication terracing within the multilayers. However, unlike these previous investigations, a single off-cut, giving rise to regular terraces, cannot be the case here, or we would expect to see two humps on either side of the specular peak, i.e. a blazed diffraction grating [22].

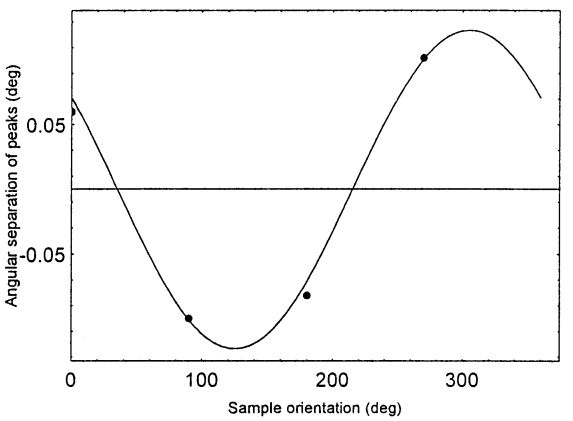

Fig. 4. Separation of the diffuse and specular peaks as a function of the azimuthal angle. The solid line is a sine function fitted to the data points.

It is interesting to note that no clear Yoneda wings appear in either experimental or simulated curves of Fig. 3. For the case of conformal roughness, the majority of the diffuse scatter through the Bragg peak comes from the buried interfaces and as the Yoneda wings arise from the enhancement of the electric field amplitude in the surface at the critical angle, these features are hidden when the majority of the scattering is from the conformal roughness of the multilayer. This effect has previously been noted experimentally and the very good agreement between the DWBA simulation and the experiment is noteworthy.

With respect to the specular peak, the angle at which the diffuse scatter rises to the mean value far from the specular peak, i.e. the position of the buried Yoneda wing, is constant for all four azimuthal settings and does not follow the sinusoidal dependence of the peak in the diffuse scatter. We also note that no change was observed in the specular curve on rotation. The coupling of the Yoneda and specular positions can be understood in the following way. As the observed diffuse scatter intensity originates from roughness in the sample, if the roughness has a preferential direction, as in the case of terracing, this will be mirrored in the diffuse scatter. In contrast, the Yoneda wings arise as an increase in diffuse scatter at the critical angles, due to an enhanced electric field at the interface at these angles. This arises as a direct consequence of the boundary matching of electromagnetic waves at the interface. These same waves govern the direction from which the specular scatter emerges and so a coupling of the positions of the specular and Yoneda wing positions occurs.

The theoretical treatment of the scattering of X-rays from terraced scatter systems has been given by several authors [21,23]. In some cases the specular scatter is said to arise from the average surface [24], while others restrict the argument to regions that are able to scatter coherently [25]. We have observed in studies of large grain alumina ceramics that the measured position of the Yoneda wings relates to the average surface density of the material. From this observation it can be deduced that the electromagnetic waves matched across the average surface within their coherence length [26]. Using this assumption, we were able to successfully model the variations in diffuse scatter. The same strategy was adopted and we see from Fig. 3 that the agreement is again excellent. This provides further support for the model of Cowley in this instance [24].

However, it proved possible to obtain quite good fits to the transverse scans through the Bragg peak for a range of correlation lengths between 1300 and 400 Å and fractal parameters between 0.2 and 0.45, there being significant coupling between the two in this region. In order to establish the uniqueness of the simulated structure, the scattering at different angles and at different wavelengths was simulated. Transverse diffuse scans taken through a Kiessig maximum and minimum at a wavelength of 1.3801 Å are shown in Fig. 5 with the best-fit simulations. Note that the Yoneda wings are well

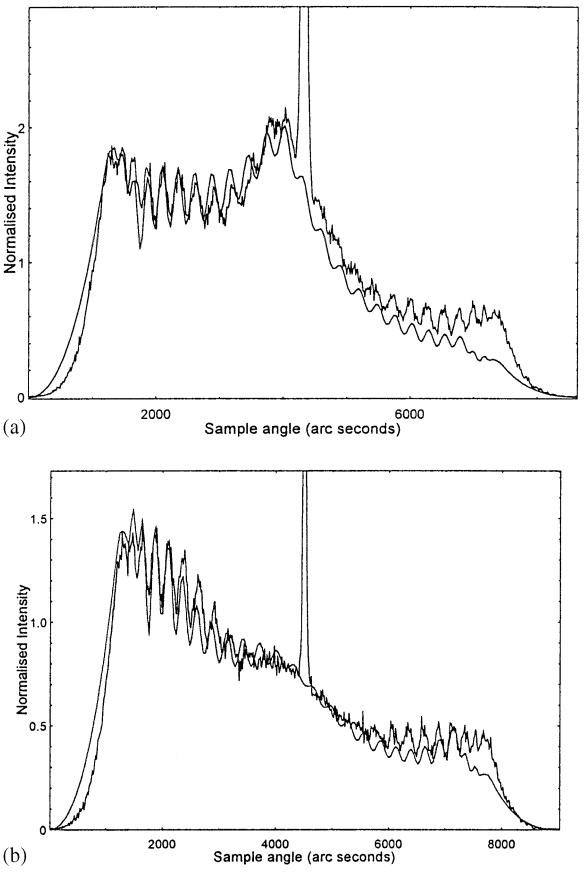

Fig. 5. Transverse scans through a Kiessig (a) maxima and (b) minimum, wavelength of 1.3801 Å.

defined. Increasing the number of transverse diffuse scans dramatically reduced the number of possible solutions and a value of $\xi = 450 \pm 50$ Å and $H = 0.28 \pm 0.05$ was found to fit six independent data sets at wavelengths of 1.3801 and 1.48 Å. To obtain a good fit to the diffuse scatter, it was necessary to assume that the ratio of correlated to uncorrelated roughness on the Cu/Co interfaces was 60 : 40.

A combination of scans in reciprocal space enables a contour map of the scattering to be produced. Such a simulated map (Fig. 6) shows that the scattering is very substantially enhanced around the q_z value corresponding to the first Bragg reflection from the superlattice. This enhancement of scattering is an interference effect that is characteristic of the presence of correlated roughness through the multilayer. When the lateral correlation length is short, these features appear much more extensive in reciprocal space [27]. Through the effect of the refractive index correction they are curved, leading to the name of "Holý bananas". In this case, however, the long correlation length restricts the scattering in the q_y direction and the enhancement occurs only close to the specular Bragg peak.

We also note that for correlated (conformal) roughness (Fig. 6a), Kiessig interference fringes occur in longitudinal off-specular scans. They are not present when the roughness on the multilayer is uncorrelated through the stack. As indicated above, the presence of such fringes in the off-specular scans in Fig. 7 is a clear indication of significant correlated roughness and the fraction can be deduced from the fringe amplitude relative to that simulated. This is found to be in the ratio 60 : 40, in agreement with the fits to the transverse diffuse scan data of Fig. 3. The interference fringes in the transverse scans of Fig. 5 do not relate to conformality in the roughness but instead arise from the interference between the incident and specularly reflected waves. Such fringes are not predicted in the Born-wave approximation but are very well simulated in the distorted-wave Born approximation. In this case, the top surface showed more correlated roughness, the ratio being 70 : 30. The ratio of correlated to uncorrelated roughness in the multilayer, determined from the amplitude of the Kiessig interference fringes and the Bragg peak in the off-specular, longitudinal scans (Fig. 7) is in good agreement.

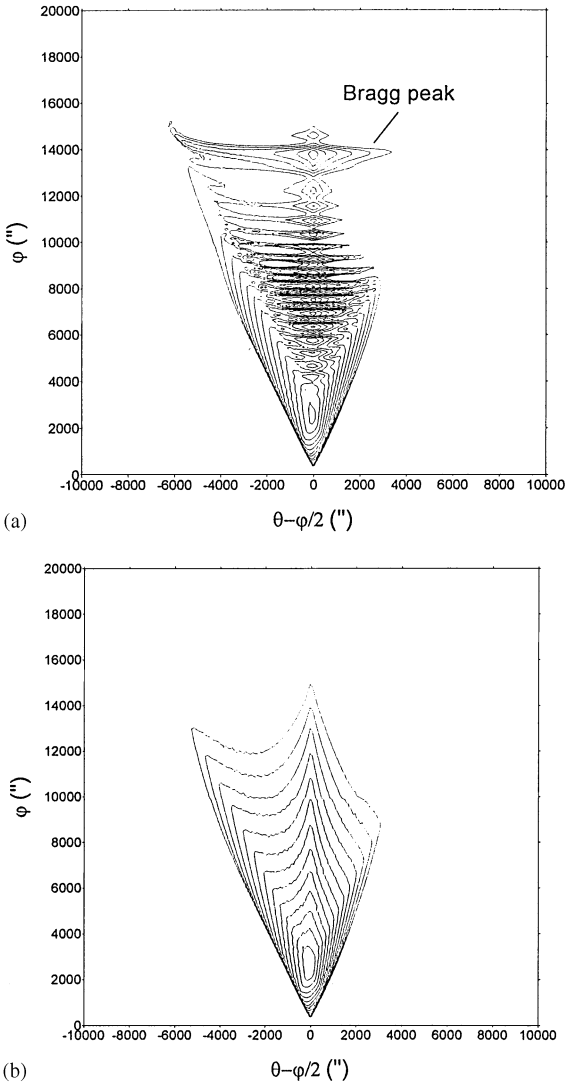

Fig. 6. Simulated reciprocal space maps of the scattering from the Co/Cu multilayer (a) with vertically correlated roughness and (b) with vertically uncorrelated roughness. The asymmetry about the origin is a result of the decreasing illuminated area as the specimen angle, θ, is increased. The neighbouring isointensity contours represent an intensity ratio of 10^2. φ is the detector angle.

However, it is still uncertain whether the sharply peaked scattering is an artefact of a figured surface, rather than genuine diffuse scatter. If the specimen

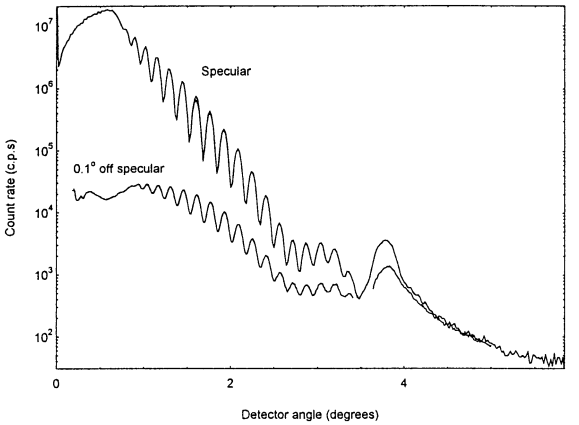

Fig. 7. Specular and off-specular longitudinal scans showing interference fringes in the diffuse scatter, characteristic of strong correlated roughness.

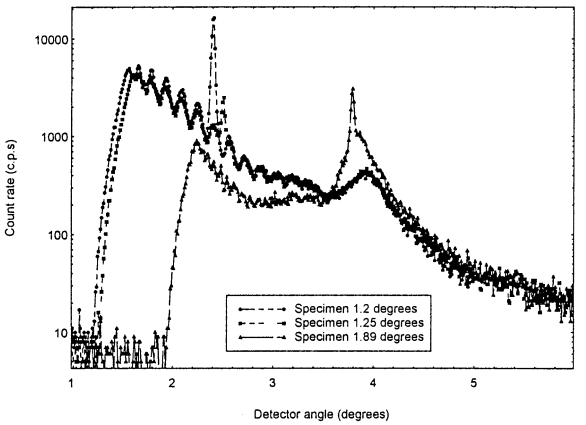

Fig. 8. Detector-only scan for three different incidence angles on the specimen.

contained a region with a moderate amount of curvature, which was misoriented with respect to the main part of the sample, a subsidiary peak would be observed that scaled with the intensity of the main specular peak and also had the angular dependence on specimen rotation seen in Fig. 4. To resolve this question, we performed scans of the detector only at three different angles of the specimen with respect to the incident beam. These are shown in Fig. 8. For the specimen set to 1.2 and 1.25°, the sharp specular peak and the diffuse peak are well separated. However, for the specimen at 1.89°, corresponding to the Bragg position, the two peaks are almost coincident in the detector scan. As illustrated in Fig. 9, for a figuring artefact, the peak separation in a detector scan will increase with the scattering vector. If the peak arises from stepping of the interfaces, the centroid of the diffuse scatter will be displaced from the specular ridge. The detector angle between cutting the specular ridge and the broad peak from the conformal roughness decreases with increasing specimen angle. As this behaviour is indeed observed, we can be confident that the peak corresponds to diffuse scatter and is not figuring.

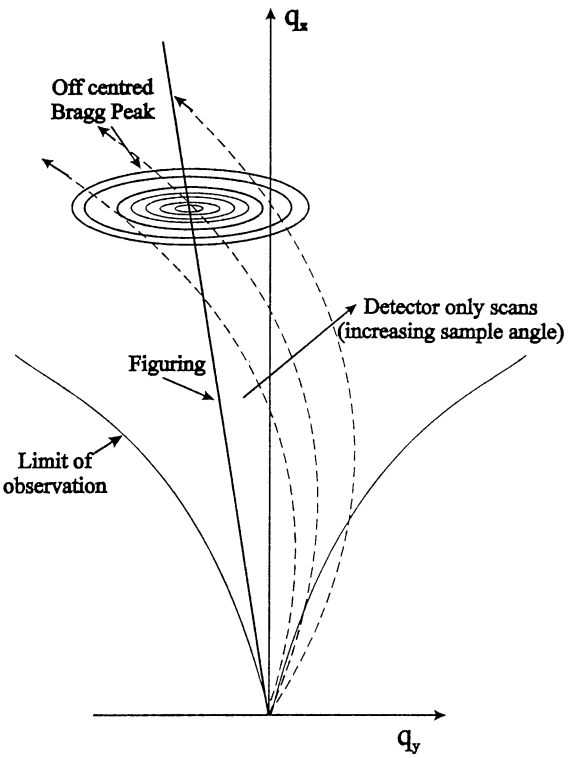

Fig. 9. Figuring and off-centred diffuse scatter displayed in reciprocal space.

Well developed interference fringes are shown in Fig. 8. These are unlike those found in transverse scans, such as Fig. 5, where interference fringes can arise from uncorrelated roughness, as the overall electric field amplitude in the specimen is modulated by the specular Kiessig fringes. In a detector-only scan, however, the incident beam remains at a fixed angle with respect to the specimen

and the electric field inside the sample remains constant throughout the scan. Thus the interference fringes correspond to coherence in the scattered wave and hence coherence in the diffuse scatter, which can only originate from correlation in the roughness for the various interfaces in the sample.

5. The validity of a self-affine model for MBE growth

Although an excellent match to a single set of parameters was found for most data, simulations of the Kiessig minimum showed a sharper peak in the diffuse scatter than that observed experimentally. We have found that a suppression of this peak can be obtained by increasing the degree of correlation between the top and bottom of the layers. As the penetration of the incident wave differs for the Kiessig maxima and minima, a variation in the degree of conformality of the roughness through the stack will result in a different best-fit under these two different conditions. Although our model enables us to specify the fraction of correlated to uncorrelated roughness at each interface, it is extremely difficult to perform such a multivariable minimisation.

In order to keep computation times reasonable for this quite complex system, it was assumed that vertical correlations extend equally over all frequencies of roughness defined within the correlation length. Thus, ignoring the optical effects of the Yoneda wings, all of the diffuse scatter in q_y is changed by the same amount on the introduction of vertical correlations in the roughness. It may be expected [28] that the shorter periods of roughness are suppressed as they propagate up through the stack. Thus, at the Kiessig minima, where the sensitivity to the near surface region is greater than at the Kiessig maxima, the centre of the transverse diffuse scan would be lowered.

Despite problems surrounding the exact mathematical description of the behaviour of MBE systems, a number of researchers have found self-affine-type scaling properties of MBE grown surfaces [29–31]. However, the "Schwoebel barrier", a potential barrier which tends to deter atoms from jumping down a step edge [29] can cause local irregularities that develop on the surface to blow up to create large mounds. These mounds are not self-affine in nature and dominate the surface profile. As a consequence, the self-affinity of the surface is destroyed. Experimentally these mounds have been observed in MBE systems [29,32,33]. However, we feel that the evidence available at this time merely proves or disproves the existence of self-affine scaling in very specific examples and this cannot be generalised to MBE grown surfaces as a whole.

In the past there have been attempts to simulate terraced surfaces by using a fractal model [19]. However, in the last year or so, it has become widely believed that a terraced surface cannot be described by such a model [34,35], due to such a surface not scaling in a self-affine way. As a result, new models are being devised such as roof, terrace, and castallation models to account for these effects [34,35]. With regard to the Co/Cu multilayers grown on silicon, a simple off-cut cannot be present for two reasons. Firstly, the diffuse scatter is symmetric on rotation of the sample by 90° about its surface normal, and secondly, such a simple model would give rise to a blazed grating effect [36]. In addition, the local tilts within this structure must be at an angle to the average sample surface. This is required so that the diffuse peak is offset from the specular position. Furthermore, there can be no periodicities within this structure, since no grating effects are seen.

One possible structure that may give rise to the observed diffuse scatter is one in which the atomic steps have bunched into regions separated by large flat terraces. Although such a surface is clearly not self-affine on a macroscopic scale, the fractal model is seen to give a reasonable fit to the experimental data. This apparent anomaly, may be resolved when consideration is given to where the bulk of the diffuse scatter is arising. It is clear that the surface is most rough in the region of the step bunching. As a result, although it is clear that the macroscopic surface is not scaling in a self-affine manner, it may be possible that on smaller length scales, within the bunches themselves, such scaling is present. Thus, the self-affine model can provide a satisfactory fit to the observed diffuse scatter from

certain microscopic regions on the sample if they dominate the diffuse scatter.

6. Conclusions

The results described here confirm our previous conclusion [9] that the peak, displaced from the specular scatter, in transverse scans of Co–Cu multilayers grown on silicon is associated with long correlation length roughness at stepped interfaces. The roughness is strongly correlated through the multilayer, giving rise to characteristic interference fringes in the diffuse scatter. We have used a DWBA theoretical model to fit the experimental data and have shown that the same set of parameters can be used for data taken under different X-ray optical conditions. While it can never be possible to have sufficiently good data to obtain a unique solution for the structural parameters by fitting to one data set, the probability of a local minimum in the difference between theory and experiment surviving a major change in experimental parameters is extremely low. We can thus be confident that the fractal model used to fit the data is a good representation of the interface and layer structure in these MBE-grown Co–Cu multilayers.

Acknowledgements

The work was supported financially by the Engineering and Physical Science Research Council through a CASE award with Daresbury Laboratory and with the UK Department of Trade and Industry through a LINK project. The Durham work was undertaken within the European Community Human and Capital Mobility Network ERBCHRXCT 930320.

References

[1] M.N. Baibich, J.M. Broto, A. Fert, F. Nguyen Van Dau, F. Petroff, P. Etienne, G. Creuzet, A. Fiedrich, J. Chazelas, Phys. Rev. Lett. 61 (1988) 2472.
[2] S.S.P. Parkin, R. Bhadra, K.P. Roche, Phys. Rev. Lett. 66 (1991) 2152.
[3] S.S.P. Parkin, Z.G. Li, D. Smith, Appl. Phys. Lett. 58 (1991) 2710.
[4] E.E. Fullerton, D.M. Kelly, J. Guimpel, I.K. Schuller, Y. Bruynseraede, Phys. Rev. Lett. 68 (1992) 859.
[5] M.E. Tomlinson, R.J. Pollard, D.G. Lord, P.J. Grundy, Zhao Chun, IEEE Trans Mag. MAG 28 (1992) 2662.
[6] K.Y. Kok, J.A. Leake, Thin Solid Films 275 (1996) 210.
[7] H. Laidler, C.I. Gregory, I. Pape, B.J. Hickey, B.K. Tanner, J Magn. Magn. Mater. 154 (1996) 165.
[8] M. Safa, B.K. Tanner, J. Magn. Magn. Mater. 150 (1995) L290.
[9] I. Pape, T.P.A. Hase, B.K. Tanner, H. Laidler, C. Emmerson, T. Shen, B.J. Hickey, J. Magn. Magn. Mater. 156 (1996) 373.
[10] B.K. Tanner, D.E. Joyce, T.P.A. Hase, I. Pape, and P.J. Grundy, Adv. X-ray Anal. 40 (1998) in press.
[11] S. Cockerton, B.K. Tanner, Adv. X-ray Anal. 38 (1995) 371.
[12] L.G. Parratt, Phys. Rev. 95 (1954) 359.
[13] V. Holý, T. Baumbach, Phys. Rev. B 49 (1994) 10668.
[14] S. Dietrich, A. Haase, Phys. Reports 260 (1995) 1.
[15] S.K. Sinha, E.B. Sirota, S. Garoff, H.B. Stanley, Phys Rev. B 38 (1988) 2297.
[16] D.K. Bowen, M. Wormington, Adv. X-ray Anal. 36 (1993) 171.
[17] M. Wormington, I. Pape, T.P.A. Hase, B.K. Tanner, D.K. Bowen, Phil. Mag. Letters 74 (1996) 211.
[18] Q. Shen, Phys. Rev. Lett. 64 (4) (1990) 451.
[19] S.K. Sinha, Physica B 198 (1994) 72.
[20] H. Zabel, Appl. Phys. Lett. 43 (1) (1983) 59.
[21] D.K.G. de Bohr, X-ray Spec. 24 (1995) 91.
[22] P. Madakson, J. Appl. Phys. 68 (5) (1990) 2121.
[23] V. Holy, Phys. Rev. B 55 (15) (1997) 9960.
[24] R.A. Cowley, Phys. Rev. B 48 (19) (1993) 14463.
[25] R. Pynn, Physica B 198, No. 1–3 (1994) 1.
[26] I. Pape, Ph.D. Thesis, Durham University, 1997.
[27] V. Holý, T. Baumbach, Phys. Rev. B 49 (1994) 10668.
[28] D.E. Savage, J. Kleiner, N. Schimke, Y.-H. Phang, T. Jankowski, J. Jacobs, R. Kariotis, M.G. Lagally, J. Appl. Phys. 69 (3) (1991) 1411.
[29] A.L. Barabasi, Fractal concepts in surface growth, Cambridge University Press, 1995.
[30] Y.P. Palasantzas, Phys. Rev. B 49 (1994) 4902.
[31] B. Lengeler, Phys. Rev. B 46 (1992) 7953.
[32] J.L. Whitehouse, Appl. Phys. Lett. 59 (1991) 3282.
[33] R.A. Cotta, Phys. Rev. Lett. 70 (1993) 4106.
[34] S.K. Sinha, Acta Physica Polonica 89 (1996) 219.
[35] V. Holy, Proc. X TOP'96, Palermo, Italy, Il Nuovo Cimento (in press).
[36] M.G. Lagally, Phys. Rev. B 50 (19) (1994) 14435.